Performance of F-DMAS beamforming with adjustable maximum spatial lag in multi-line transmission ultrasound imaging

Performance of F-DMAS Beamforming with Adjustable Maximum Spatial Lag in Multi-Line Transmission Ultrasound Imaging

Giulia Matrone
Dept. of Electrical, Computer and Biomedical Engineering
University of Pavia
Pavia, Italy
giulia.matrone@unipv.it

Alessandro Ramalli
Dept. of Cardiovascular Sciences
KU Leuven
Leuven, Belgium

Jan D'hooge
Dept. of Cardiovascular Sciences
KU Leuven
Leuven, Belgium

Piero Tortoli
Dept. of Information Engineering
University of Florence
Florence, Italy

Giovanni Magenes
Dept. of Electrical, Computer and Biomedical Engineering
University of Pavia
Pavia, Italy

***Abstract*—In Multi-Line Transmission (MLT) ultrasound imaging, high frame-rate is achieved by the simultaneous transmission of multiple focused beams along different directions. Image contrast is potentially degraded by cross-talk artifacts that, however, can be successfully attenuated e.g. by Filtered-Delay Multiply and Sum (F-DMAS) beamforming. F-DMAS is based on the computation of the autocorrelation of the aperture in reception, which is related to the spatial-coherence (SC) of backscattered signals. SC in turn is affected by the two-way beam shape. Since MLT has a major effect on SC, a new F-DMAS formulation, called Short-Lag (SL) F-DMAS, is here proposed that allows setting the maximum lag (MLAG) between the echo signals used in the correlation operation on which image reconstruction is based. The performance of the new approach in MLT imaging is assessed through simulations. Results show that the smaller the MLAG value, the better the spatial resolution and speckle uniformity. On the other hand, contrast worsens due to increasing crosstalk artifacts. This analysis thus provides valuable indications to select the MLAG (thus, a certain trade-off between contrast, resolution and speckle-SNR) based on the specific requirements for a given application.**

Keywords—non-linear beamforming, delay multiply and sum, high frame-rate, multi-line transmission, short lag spatial coherence, ultrasound imaging

I. Introduction

The concept of spatial coherence of backscattered signals [1] has recently been exploited to develop several image formation techniques, enabling high quality ultrasound imaging with improved clutter rejection, spatial resolution and contrast. Such methods include for example Short Lag Spatial Coherence (SLSC) imaging [2], phase and sign coherence beamforming [3], coherence factor weighting [4], and Filtered-Delay Multiply and Sum (F-DMAS) beamforming [5]. In particular, some of the authors have worked on this last technique, which was proven to successfully improve image contrast resolution in several applications, including high frame rate imaging with plane-waves [6] and multi-line transmission (MLT) [7].

The F-DMAS algorithm [5] is based on the computation of the spatial correlation of backscattered signals received by the N-element aperture in reception (RX). Basically, it consists in focusing these radiofrequency (RF) signals, coupling them by making all possible combinations, and then multiplying each pair of signals to generate $(N^2\text{-}N)/2$ outputs, which are finally summed and band-pass filtered around the second harmonic frequency. In this process, cross-multiplications are made between signals at different spatial lags, from 1 to N-1, where N is the number of RX aperture elements.

In this work we study how F-DMAS beamforming behaves when an upper limit is set to the maximum lag between the signals, i.e. only part of the possible signal couples are considered in the correlation operation, and the performance of this version of the algorithm (called Short-Lag (SL) F-DMAS [8]) is analyzed.

In the study we focus on the application of SL F-DMAS in high frame-rate ultrasound imaging with MLT. The latter technique in fact consists in transmitting multiple beams simultaneously to increase the frame-rate by a factor equal to the number of such beams [9]. Interferences among them however occur, which generate crosstalk artifacts in the final image, worsening its contrast [10, 11].

Since in MLT imaging the pulse-echo beam shape is affected by this phenomenon, which in turn reduces spatial coherence of echo signals, we investigate how such reduction influences the performance of F-DMAS. Results of point-target and phantom simulations are used to evaluate image resolution, contrast and speckle uniformity achieved by the algorithm in this particular case, hence providing further insights on the dependence of F-DMAS behavior on the spatial coherence of the backscattered echoes.

This work was partially supported by the University of Pavia under the Blue Sky Research project MULTIWAVE. A. Ramalli was supported by the European Union's Horizon 2020 research and innovation programme under the Marie Skłodowska-Curie grant agreement No 786027 (ACOUSTIC project).

DOI: 10.1109/ULTSYM.2018.8579761

II. Materials and Methods

A. Short Lag F-DMAS Beamforming

The first step of the SL F-DMAS algorithm consists in delaying the received signals as in Delay and Sum (DAS). Then, signals are amplitude-rescaled by means of a signed square root operation and coupled, by making all possible combinations among them up to a certain spatial lag (L). If we use for example an N-element RX aperture, i.e. N backscattered RF signals $s_n(t)$ with $n = 1 \ldots N$, and we select L = MLAG as the maximum spatial-lag value to be considered, then the SL F-DMAS formulation is the following [8]:

$$z_{sl-fdmas}(t) = \sum_{L=1}^{MLAG} \sum_{n=1}^{N-L} sign(s_n(t)s_{n+L}(t)) \cdot \sqrt{|s_n(t)s_{n+L}(t)|} \quad (1)$$

SL F-DMAS becomes equivalent to F-DMAS when MLAG=N-1, i.e. all the received RF signals are combinatorially coupled and multiplied [5, 8].

The beamformer output signal $z_{sl\text{-}fdmas}$ is in the end band-pass filtered around the second harmonics. To obtain the final image, envelope-detection, normalization and log-compression are subsequently applied.

B. Multi-Line Transmission

The ultrasound pulse-echo response can be generally computed by convolving the TX and RX array responses, h_{TX} and h_{RX}:

$$\begin{cases} h_{TX}(u) = \mathrm{sinc}(\frac{p_x u}{\lambda}) \sum_{i=1}^{N_B} \mathrm{sinc}[\frac{Np_x}{\lambda}(u - \sum_{j=-\infty}^{+\infty} \frac{j\lambda}{p_x} - u_i^{TX})] \\ h_{RX}(u) = \mathrm{sinc}(\frac{p_x u}{\lambda}) \mathrm{sinc}[\frac{Np_x}{\lambda}(u - \sum_{j=-\infty}^{+\infty} \frac{j\lambda}{p_x} - u^{RX})] \end{cases} \quad (2)$$

where $u=sin(\theta)$ and θ is the beam steering angle, u_{TX} and u_{RX} refer to the steering direction of the TX and RX beam, respectively, p_x is the array pitch and λ is the wavelength [8, 12].

In standard B-mode imaging, each time a scan line is acquired sequentially by transmitting and receiving a single beam (i.e. Single Line Transmission, SLT), thus N_B = 1. In MLT imaging, instead, multiple (i.e. N_B) TX beams are transmitted simultaneously along different directions, thus a different pulse-echo beam shape is obtained compared to SLT. The excitation pulse is computed by summing up N_B delayed pulses that would be used in the SLT case to focus along the N_B TX directions. In this way, also the pulse-echo beam shape changes and the so-called crosstalk artifacts [10] arise in the image, due to inter-beam interferences, worsening the contrast. On the other hand, the frame-rate improves by N_B times, as less TX events are required to acquire all the lines of the image.

C. Simulation setup

Field II [13, 14] simulations in Matlab were carried out to generate both images of a point-scatterer and of a phantom with an anechoic cyst inclusion.

A 2 MHz, 64-element phased array was modeled, with a 0.34 mm pitch and 12 mm element height. A 90° image sector was scanned simulating 192 scan lines. The TX focus was set at 70 mm depth while dynamic focusing was implemented in RX. The excitation signal was a 2-cycle sinusoidal burst with Hanning tapering at 2 MHz. Two different configurations were considered, i.e. standard SLT and transmitting 4 beams simultaneously (4-MLT).

A point scatterer was placed at (x, z) = (0, 70) mm, in order to obtain the point spread function (PSF) image of the system and hence evaluate the lateral resolution, i.e. the PSF main lobe width at -6 dB. Then, phantom images were simulated by modeling a tissue phantom with a 10-mm-diameter anechoic cyst centered at (x, z) = (0, 70) mm, and contrast ratio (CR), contrast-to-noise ratio (CNR) and speckle signal-to-noise ratio (sSNR) were measured at the focal depth (as defined in [5]).

The performance achieved by SL F-DMAS at different MLAG values, including standard F-DMAS (i.e. MLAG=63), was compared to that of DAS with Tukey RX apodization. Tukey TX apodization (with α=0.5) was applied in TX in both cases, in order to suppress TX crosstalk artifacts (as proposed in [10]) and to evaluate the RX crosstalk rejection capabilities of the two beamformers. Besides, the F-DMAS final band-pass filter was set between 1.5-7 MHz.

III. Results

The plots represented in Fig. 1 give an overview of the performance achieved by SL F-DMAS considering different MLAG values.

The first panel on the left refers to the trend of lateral resolution. As expected, the lateral resolutions achieved in SLT and 4-MLT images are comparable, since MLT crosstalk does not affect the main lobe lateral width. However, SL F-DMAS performs better than DAS for every MLAG: in particular, the smaller the MLAG value, the better the resolution. The worst value is obtained with standard F-DMAS (MLAG=63), i.e. 2.4 mm vs. 3 mm obtained with DAS, as reported in Table I.

Qualitatively, the PSF images in Fig. 2 confirm this worsening trend of resolution with increasing values of MLAG; on the other hand, they also show an opposite trend of the side-lobe level, which improves as MLAG becomes higher. This in turn accounts for an improvement of contrast resolution performance.

In the central and right panels of Fig. 1, the CR and CNR trends are represented, respectively. The former shows that a better contrast can be achieved with SL F-DMAS as MLAG increases, which becomes higher than that of DAS at MLAG=13 for SLT or MLAG=32 for 4-MLT imaging. With standard F-DMAS, the CR is ~16 dB and ~8 dB higher (in absolute value) than that of DAS for SLT and 4-MLT, respectively (see Table II).

CNR and sSNR are lower with SL F-DMAS than with DAS, for all MLAG values (Fig. 1, right panel). At shorter lags, the SL F-DMAS CNR is slightly worse, but in general it has an almost constant trend around 1.8 and 1.4 in SLT and 4-MLT, respectively; for DAS instead, CNR is 2.2. Also the sSNR undergoes small variations, in this case worsening as

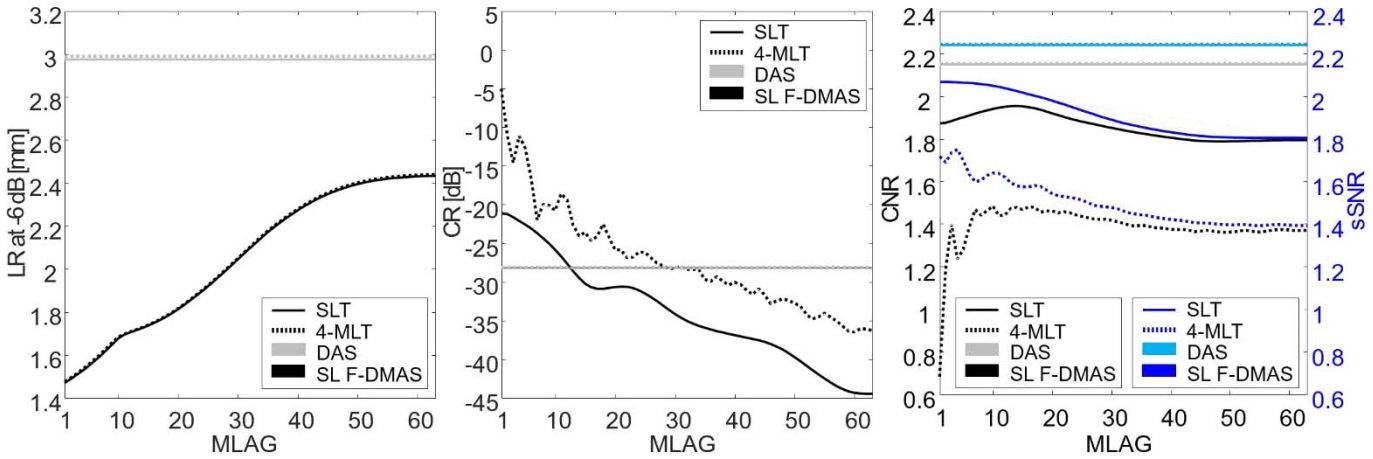

Fig. 1. Comparison of performance parameter trends obtained with different imaging configurations in simulations: lateral resolution (LR) at -6 dB (left panel), CR (central panel), CNR and sSNR (right panel). Line color refers to the beamforming technique implemented (DAS with Tukey RX apodization or SL F-DMAS), while line pattern (solid or dotted) indicates the acquisition modality (SLT or 4-MLT).

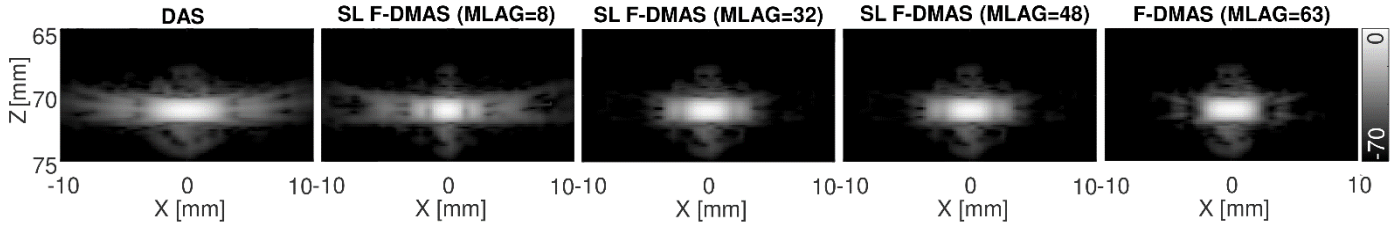

Fig. 2. Simulated 4-MLT images of the PSF at 70 mm depth obtained with DAS plus Tukey RX beamforming, SL F-DMAS with different MLAG values (MLAG = 8, 32, 48) and standard F-DMAS (MLAG = 63). Images are represented over a 70 dB dynamic range (log scale).

MLAG increases. Shorter MLAGs worsen the CNR but enhance sSNR, since cross-talk rejection is weakened but speckle uniformity is improved. These trends are confirmed by the cyst-phantom images in Fig. 3, obtained with SL F-DMAS at different MLAGs for 4-MLT imaging. The CR, CNR and sSNR measured on these images (and also on SLT ones, for reference) are reported in Table II.

By looking at the cysts in Fig. 3 it is clearly visible that resolution is higher for MLAG=8, as the cyst diameter is almost equal to the real one; however, the area inside it is degraded by clutter and crosstalk artifacts, which make contrast low. When MLAG increases, up to 63, the cyst becomes darker, but its diameter slightly reduces (the smallest diameter is in any case that obtained with DAS). At the same time, several dark areas appear in the speckle background, partially worsening its uniformity.

IV. Conclusion

This paper investigates more in depth the behavior of the F-DMAS beamformer, by proposing a different formulation called SL F-DMAS, which is aimed at understanding the impact of spatial coherence of backscattered echoes on the algorithm performance. In particular, the analysis is focused on high frame-rate imaging with MLT, where the use of multiple TX beams has an impact on the pulse-echo beam shape and, in turn, on signals spatial coherence.

Simulated images are obtained by using only RF-signal couples below a certain maximum spatial lag in the SL F-DMAS cross-multiplication procedure, in order to evaluate contrast, resolution and speckle uniformity at different MLAG values as compared to DAS. Results show how SL-FDMAS can be tuned to achieve different imaging performances, i.e. a certain trade-off between the above-mentioned image-quality parameters. Shorter lags allow improving resolution and speckle uniformity, sacrificing contrast; on the opposite, high MLAG values improve contrast, but lower resolution and speckle quality. Nevertheless, in any case the CR and resolution obtained with SL F-DMAS are better than those achievable with DAS and Tukey RX apodization, both in SLT and MLT imaging.

In conclusion, SL F-DMAS provides valuable indications to select the MLAG based on the specific application requirements.

TABLE I. PSF Main Lobe Width (Lateral Resolution)

Method	Main Lobe Width at -6 dB [mm]	
	SLT	***4-MLT***
DAS	2.97	2.99
SL F-DMAS (MLAG=8)	1.62	1.63
SL F-DMAS (MLAG=32)	2.10	2.10
SL F-DMAS (MLAG=48)	2.38	2.39
F-DMAS	2.43	2.44

In the DAS case, Tukey RX apodization is applied.

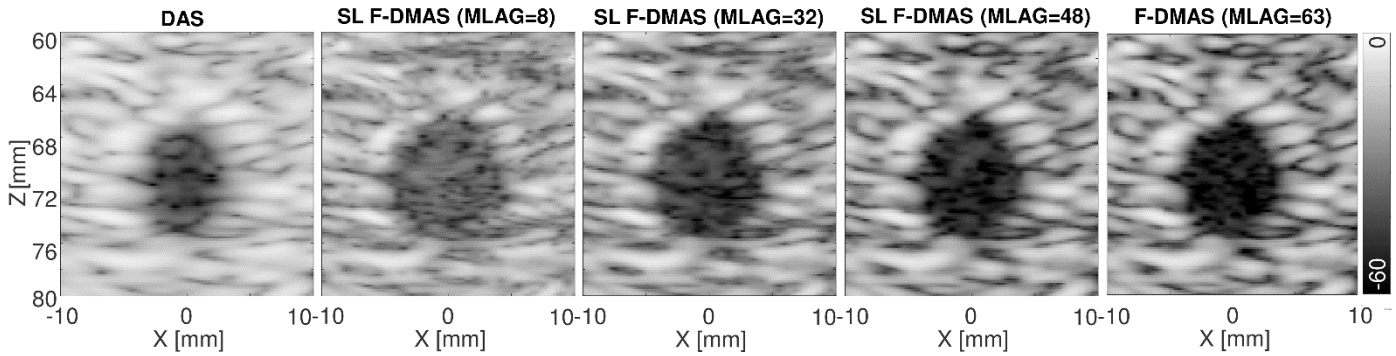

Fig. 3. Simulated 4-MLT images of the cyst phantom obtained with DAS plus Tukey RX beamforming, SL F-DMAS with different MLAG values (MLAG = 8, 32, 48) and standard F-DMAS. Images are represented over a 60 dB dynamic range (log scale).

TABLE II. CR, CNR AND sSNR OF CYST PHANTOM IMAGES

Method	**CR [dB]**		**CNR**		**sSNR**	
	SLT	***4MLT***	***SLT***	***4MLT***	***SLT***	***4MLT***
DAS	-28.11	-28.16	2.15	2.15	2.24	2.25
SL F-DMAS (MLAG=8)	-24.38	-20	1.93	1.44	2.06	1.61
SL F-DMAS (MLAG=32)	-35.03	-28.41	1.84	1.40	1.87	1.46
SL F-DMAS (MLAG=48)	-38.73	-32.23	1.79	1.37	1.81	1.40
F-DMAS	-44.41	-36.31	1.79	1.37	1.80	1.39

In the DAS case, Tukey RX apodization is applied.

REFERENCES

[1] R. Mallart and M. Fink, "Adaptive focusing in scattering media through sound-speed inhomogeneities: the Van Cittert Zernike approach and focusing criterion," *J. Acoust. Soc. Am.*, vol. 96, no. 6, pp. 3721-3732, 1994.

[2] M. A. Lediju, G. E. Trahey, B. C. Byram, J. J. Dahl, "Short-Lag Spatial Coherence of backscattered echoes: imaging characteristics," *IEEE Trans. Ultrason. Ferroelectr. Freq. Control*, vol. 58, no. 7, pp. 1377-1388, 2011.

[3] J. Camacho, M. Parrilla, C. Fritsch, "Phase coherence imaging," *IEEE Trans. Ultrason., Ferroelectr., Freq. Control*, vol. 56, no. 5, pp. 958-974, 2009.

[4] P. -C. Li and M. -L. Li, "Adaptive imaging using the generalized coherence factor," *IEEE Trans. Ultrason. Ferroelectr. Freq. Control*, vol. 50, no. 2, pp. 128-142, 2003.

[5] G. Matrone, A. S. Savoia, G. Caliano, G. Magenes, "The Delay Multiply and Sum beamforming algorithm in ultrasound B-mode medical imaging," *IEEE Trans. Med. Imag.*, vol. 34, no. 4, pp. 940-949, 2015.

[6] G. Matrone, A. S. Savoia, G. Magenes, "Filtered Delay Multiply And Sum Beamforming in Plane-Wave Ultrasound Imaging: Tests on Simulated and Experimental Data," *Proc. IEEE International Ultrasonics Symposium, Tours*, France, 2016.

[7] G. Matrone, A. Ramalli, A. S. Savoia, P. Tortoli, G. Magenes, "High Frame-Rate, High Resolution Ultrasound Imaging With Multi-Line Transmission and Filtered-Delay Multiply And Sum Beamforming," *IEEE Trans. Med. Imag.*, vol. 36, no. 2, pp. 478-486, 2017.

[8] G. Matrone and A. Ramalli, "Spatial Coherence of Backscattered Signals in Multi-Line Transmit Ultrasound Imaging and Its Effect on Short-Lag Filtered-Delay Multiply and Sum Beamforming", *Applied Sciences*, vol. 8, no. 4, pp. 486-500, 2018.

[9] R. Mallart and M. Fink, "Improved imaging rate through simultaneous transmission of several ultrasound beams," *Proc. SPIE*, 1992, vol. 1773, pp. 120-130.

[10] L. Tong, H. Gao, J. D'hooge, "Multi-transmit beam forming for fast cardiac imaging-A simulation study," *IEEE. Trans. Ultrason. Ferroelectr. Freq. Control*, vol. 60, no. 8, pp. 1719-1731, 2013.

[11] A. Ramalli, A. Dallai, F. Guidi, L. Bassi, E. Boni, L. Tong, G. Fradella, J. D'hooge, and P, Tortoli, "Real-time high frame rate cardiac B-Mode and tissue Doppler imaging based on multiline transmission and multiline acquisition," IEEE. Trans. Ultrason., Ferroelectr., Freq. Control, 2018, DOI: 10.1109/TUFFC.2018.2869473.

[12] T. L. Szabo, *Diagnostic Ultrasound Imaging: Inside Out*. New York, NY: Elsevier Academic Press, 2004.

[13] J. A. Jensen and N. B. Svendsen, "Calculation of pressure fields from arbitrarily shaped, apodized, and excited ultrasound transducers," *IEEE Trans. Ultrason. Ferroelectr. Freq. Control*, vol. 39, no. 2, pp. 262-267, 1992.

[14] J. A. Jensen, "Field: a program for simulating ultrasound systems," *Med. Biol. Eng. Comput.*, vol. 34, pp. 351-353, 1996.